

# A Numerical study of high Rayleigh number thermal convection in shallow cavities

P.Wang and R.D.Ferraro

Jet Propulsion laboratory

California Institute of Technology

## Abstract

Two-dimensional convective flows in shallow cavities with adiabatic horizontal boundaries and driven by differential heating of the two vertical end walls, are studied over a range of Rayleigh numbers  $R_1$ , and numerical results are obtained for air in the nonlinear end zone on parallel computing systems. Boundary-layer structure and a small eddy on the streamline field near the lower cold corner occur at  $R_1 \approx 6000$ . At  $R_1 \approx 40000$ , flow separation is observed for the first time in a numerical simulation on the bottom near the cold wall for the end-zone problem, and a jet-like structure is formed. A detailed temporal evolution of the flow at  $R_1 = 40000$  is also presented.

## Nomenclature

$h$  height of cavity

$l$  length of cavity

$L = l/h$  aspect ratio of cavity

$Nu$  Nusselt number

$R$  Rayleigh number

$R_1$  scaled Rayleigh number

$\bar{T}, T$  non-dimensional temperature

$x, z$  non-dimensional coordinates

$u, w$  non-dimensional velocity components

## Greek symbols

$\beta$  coefficient of thermal expansion

$\bar{\psi}, \psi$  non-dimensional stream function

$\kappa$  thermal diffusivity

$\nu$  kinematic viscosity

$\sigma$  Prandtl number

$\bar{\omega}, \omega$  non-dimensional vorticity function

# 1 Introduction

Flows driven by lateral heating in shallow cavities are of interest in relation to many applications in engineering: the production of crystals by the gradient-freeze technique, cooling systems for nuclear reactors, and the dispersion of pollutants in river estuaries. Experimental investigations of cavity flows driven by lateral heating have been reported in [14] [17] and [15]. In general, these flows consist of a main circulation in which fluid rises at the hot wall, sinks at the cold wall, and travels laterally across the intervening core region. A typical model of convection driven by a lateral thermal gradient consists of a two dimensional rectangular cavity with the two vertical end walls held at different constant temperatures, and the flow structure only depends on three parameters: Rayleigh number  $R$ , Prandtl number  $\sigma$ , and aspect ratio  $L$  (length/height). Numerical studies for these flows have been carried out by Bejan and Tien [4], and Drummond and Korpela [8].

For a shallow cavity ( $L \rightarrow \infty$ ) and Rayleigh numbers  $R \ll L$  the flow is dominated by conduction and consists of a Hadley cell driven by the constant horizontal temperature gradient set up between the end walls. Nonlinear convective effects first become significant at the ends of the cavity where the flow is turned when  $R_1 = R/L = O(1)$ . Hart [12] found that for small  $\sigma$  the Hadley cell is susceptible to a variety of instabilities. For Rayleigh numbers greater than a critical value  $R_1 = R_{1c}(\sigma)$  the parallel core flow is destroyed and replaced by stationary multiple cells [10]. The stationary transverse mode of instability actually forms an integral part of the basic steady motion in the cavity, appearing as an imperfect bifurcation of the nonlinear flow in the end regions. Their existence was confirmed by numerical simulation of the end-zone flow at low Prandtl numbers in [13] and [19]. Solutions of the appropriate eigenvalue problem ([10]) suggest that in the case of thermally insulated horizontal boundaries this type of behaviour is relevant for Prandtl numbers  $\sigma \leq 0.12$  and

the ensuing motion is then difficult to treat analytically because nonlinear effects become important throughout the cavity for  $R_1 > R_{1c}(\sigma)$ . For larger Prandtl numbers, the asymptotic structures of the end-region solution as  $RI \rightarrow \infty$  had been discussed by Daniels [5], and numerical solutions have been obtained for the end-region flow for several different Prandtl numbers and for a range of values of the scaled Rayleigh number  $R/L$  by Wang and Daniels [20] [21]. As the Rayleigh number increases, the extent of the end-zone increases and as  $RI \rightarrow \infty$  a complicated asymptotic structure develops. In the end zone near the cold wall the structure involves the formation of a thermally-driven vertical boundary layer at the wall which entrains fluid and conveys it to the bottom corner of cavity where it is expelled into the form of a horizontal wall jet studied by Daniels and Gargaro [6]. As the jet diffuses there is a second stage of evolution where both buoyancy and the effect of an inviscid recirculation in the main part of the end zone come onto play [7]. But there are no numerical solutions for the end zone for very high Rayleigh numbers and experiments have only been done for small aspect ratios. For time-dependent thermally-driven shallow cavity flows, the temporal evolution is studied by Daniels and Wang [9] for the nonlinear region where Rayleigh number  $R$  based on cavity height is of the same order of magnitude as the aspect ratio  $L$ . For a certain class of initial conditions the evolution is found to occur over two non-dimensional timescales, of order one and of order  $L^2$ . Analytical solutions for the motion throughout most of the cavity are found for each of these timescales and numerical solutions are obtained for the nonlinear time-dependent motion in the regions near each lateral wall. But for high Rayleigh numbers time-dependent shallow cavity flow, more work needs to be considered.

The present study investigates high Rayleigh number convective flows in end-zones of cavities with thermally insulated horizontal surfaces and endwalls held at different fixed temperatures. The

problem formulation, the core solution, and the end-zone problem are given in Section 2. The numerical scheme and parallel computing techniques for the end-zone problem are discussed in Section 3. The steady-state solution for different Rayleigh numbers are presented in Section 4 and in Section 5 the evolution of time-dependent flow is discussed and numerical results are given for a high Rayleigh number. Finally, conclusions are outlined in Section 6.

## 2 Formulation, core solution and end-zone structure

The flow domain is a rectangular cavity of length 1 and height  $h$ . The end wall at  $x = L = 1/h$  is maintained at a constant temperature  $A_1$  in excess of that at  $x = 0$  and the two horizontal walls  $z = 0$  and  $z = 1$  are perfectly insulated. Subject to the Oberbeck-Boussinesq approximation, the governing equations of the time-dependent motions in non-dimensional form as

$$\sigma^{-1} \left( \frac{\partial \bar{\omega}}{\partial t} + J(\bar{\omega}, \bar{\psi}) \right) = \nabla^2 \bar{\omega} + R \frac{\partial \bar{T}}{\partial x}, \quad (1)$$

$$\nabla^2 \bar{\psi} = -\bar{\omega}, \quad (2)$$

$$\frac{\partial \bar{T}}{\partial t} + J(\bar{T}, \bar{\psi}) = \nabla^2 \bar{T}, \quad (3)$$

for the vorticity  $\bar{\omega}$ , stream function  $\bar{\psi}$  and temperature  $\bar{T}$ , and the Prandtl number  $\sigma$  and the Rayleigh number  $R$  are defined by

$$\sigma = \frac{\nu}{\kappa}, \quad R = \frac{g\beta\Delta T h^3}{\kappa\nu} \quad (4)$$

where  $g$  is the acceleration due to gravity, and  $\nu, \kappa$  and  $\beta$  are the kinematic viscosity, thermal diffusivity and coefficient of thermal expansion respectively. The boundary conditions on the rigid walls of the cavity are

$$\bar{\psi} = \frac{\partial \bar{\psi}}{\partial x} = \bar{T} = 0 \quad \text{on} \quad x = 0, \quad (5)$$

$$\bar{\psi} = \frac{\partial \bar{\psi}}{\partial x} = 0, \quad \bar{T} = 1 \quad \text{on} \quad x = L, \quad (6)$$

and the rigid horizontal surfaces are assumed to be insulating so that

$$\bar{\psi} = \frac{\partial \bar{\psi}}{\partial z} = \frac{\partial \bar{T}}{\partial z} = 0 \quad \text{on} \quad z = 0, 1, \quad (7)$$

and the above governing equations and boundary conditions are consistent with Gill's [11] centrosymmetric properties

$$\left. \begin{aligned} \bar{\psi}(x, z, t) &= \bar{\psi}(L - x, 1 - z, t), \\ \bar{T}(x, z, t) &= 1 - \bar{T}(L - x, 1 - z, t) \\ \bar{\omega}(x, z, t) &= \bar{\omega}(L - x, 1 - z, t) \end{aligned} \right\} \quad (8)$$

which allow only one half of the flow domain to be considered.

The formal asymptotic structure of the steady flow in a shallow cavity where  $L \gg 1$  and  $R_1 = R/L = O(1)$  is studied by Daniels et al [10]. Throughout most of the cavity (the core region) the flow is dominated by the lateral conduction associated with a Hadley circulation, so that

$$\bar{T} = \xi + L^{-1} \left\{ \left( \xi - \frac{1}{2} \right) c_1(R_1, \sigma) + R F'(z) \right\} + O(L^{-2}) \quad (9)$$

and

$$\bar{\psi} = R \left\{ \left[ \xi - \frac{1}{2} \right] c_1(R_1, \sigma) \right\} F'(z) + O(L^{-2}) \quad (10)$$

as  $L \rightarrow \infty$ , where  $\xi = \frac{x}{L}$ ,

$$F(z) = \frac{z^5}{120} - \frac{1}{48} z^4 + \frac{1}{72} z^3 - \frac{1}{1440} \quad (11)$$

and  $C_1(R, \sigma)$  is a constant contribution determined by matching with solutions near the end wall.

Near the cold wall, the solution adjusts to the boundary conditions (5) in a square zone where

$$x, z = 0(1),$$

$$\left. \begin{aligned} \bar{T} &= L^{-1}T(x, z, t) + \dots \\ \bar{\psi} &= \psi(x, z, t) + \dots \\ \bar{\omega} &= \omega(x, z, t) + \dots \end{aligned} \right\} (L \rightarrow \infty), \quad (12)$$

and substitution into (1)-(3) indicates that a steady-state solution of the system

$$\sigma^{-1} \left( \frac{\partial \omega}{\partial t} + J(\omega, \psi) \right) = \nabla^2 \omega - R_1 \frac{\partial T}{\partial x}, \quad (13)$$

$$\nabla^2 \psi = -\omega, \quad (14)$$

$$\frac{\partial T}{\partial t} + J(T, \psi) = \nabla^2 T, \quad (15)$$

is required. From (5-7) these equations are to be solved subject to

$$\psi = \frac{\partial \psi}{\partial z} = \frac{\partial T}{\partial z} = 0 \quad \text{on} \quad z = 0, 1, \quad (16)$$

$$\psi = \frac{\partial \psi}{\partial x} = T = 0 \quad \text{on} \quad x = 0, \quad (17)$$

and to match with the core solution

$$\psi \rightarrow R_1 F'(z), \quad T \sim x + c + R_1 F(z) \quad (x \rightarrow \infty). \quad (18)$$

The core temperature is determined to order  $L^{-1}$  through the matching requirement

$$C_1 = -2c \quad (19)$$

but the value of  $c$  itself can only be determined by solving the end-zone problem (13)-(19). At low Prandtl numbers ( $\sigma < 0.12$ ), the behaviour (18) is only possible for values of  $R_1$  less than a critical value  $R_{1c}$  ([13], [20]), but otherwise steady-state solutions are expected to exist for any value of  $R_1$ . The aim of the present work is to determine such solutions numerically for high Rayleigh numbers with  $\sigma > 0.12$ .

### 3 Numerical scheme and parallel computing techniques for the end-zone problem

A finite difference method is considered for the system (13)-(19). The explicit Dufort-Frankel scheme is used for the vorticity equation (13) and the heat equation (15), which has second order accuracy, and the numerical stability is achieved by a Courant condition. The Arakawa's scheme is for the convection terms  $J(\omega, \psi)$  and  $J(T, \psi)$ , which has been proven suitable for natural convective flow problems ([1], [19]). The Poisson equation (14) is solved by using a fast multigrid method (Brandt [3]) with a complete V-Cycle scheme on four-level grids and Successive Over-Relaxation as the smoother.

The outer form (18) at  $x = \infty$  is handled by a finite truncation of  $x$  so that the conditions

$$\psi = R_1 F(z), \frac{\partial T}{\partial x} = 1 \quad (20)$$

are applied in the computation domain as  $x = x_\infty < \infty$ . It is then necessary to ensure that  $x_\infty$  is chosen sufficiently large that the computed solution does indeed approximate the actual solution of (13)-(19). More details about an e-folding decay length of the end zone are given in [10] using eigenvalue analysis, which provide a proper scale for choosing the outer boundary of the computational domain so the parallel core flow is matched by the end zone flow. The whole computation of the above problem is carried out on powerful parallel computing systems, and an efficient parallel code is designed for large Rayleigh numbers and aspect ratios by using domain decomposition techniques. A 2D original fine mesh and its derived coarse meshes are partitioned into blocks of consecutive columns and distributed onto a linear array of processors (Figure 1). Since a large aspect ratio is considered, the above partition is optimal as it minimizes the interprocessor

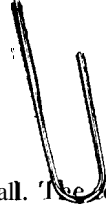


communication and maximizes the computing on each node. But the number of processors that should be used varies according to the problem to be solved. In general, a good parallel code should have a balanced computational load on each node, the independent of computing nodes, and minimize internode communication. Focusing these techniques, a parallel code for the end zone problems of natural convective flows has been implemented on the 1 ntel Paragon, Intel Touchstone Delta, and Cray T3D systems. A detailed description of the numerical scheme and parallel computing techniques is presented in Wang and Ferraro [22].

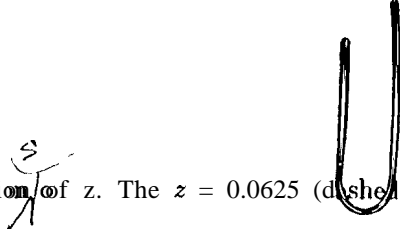
→ sentence  
reword  
more

#### 4 Steady-state solutions

Numerical solutions are obtained for a range of Rayleigh numbers  $R_1$  varying from 6000 to 40000 with  $\sigma = 0.733$ . Different truncation values  $x_\infty$  of the end zone near the cold wall have been used for different Rayleigh numbers. Most computations are carried out by using 16, 32, and 64 processors, and the choice of numbers of processors depends on the grid size used. The time step  $\Delta t$  is restricted by spatial and Rayleigh numbers, varying from  $10^{-3}$  to  $10^{-5}$  for  $R_1$  ranging from 6000 to 40000. Since an explicit scheme is used for vorticity and temperature, at each time step only one linear system derived from the Poisson equation needs to be solved, and a parallel multigrid solver has been efficiently used for this problem. For each pair of  $R_1$  and  $u$ , contour plots of the stream function, vorticity, and temperature are displayed. Figures 2 – 5 illustrate detailed contour plots for  $6000 < R_1 \leq 40000$ , which show the influence of  $R_1$  on the flow structure. When  $R_1 = 6000$ , a vertical thermal boundary layer is formed on the cold wall, and a small eddy occurs in the streamline field near the lower cold corner. At the higher Rayleigh numbers, the vertical boundary layer is much thinner, and the strongest horizontal temperature gradients are set up near the top corner of the



cold wall, where there is vigorous convection down the wall. The eddy gradually moves further down to the lower cold corner, and at  $R_1 = 25000$  more than one eddy is observed near the boundary area. When  $R_1$  is increased to 40000, the flow structure becomes much more complicated, and a jet-like structure is set up. Near the bottom corner of the cold wall, several small eddies can be clearly identified. Daniels and Gargaro [6] have discussed the thermal wall jet by using asymptotic and numerical methods for solving a similar vertical boundary layer equation there they described an initial structure of the jet and its subsequent diffusion at large distances downstream for a class of initial velocity and temperature profiles relevant to intrusion jets observed in certain thermal cavity flows. In Figure 6, a strong vorticity source at the lower corner is also shown at the contours of vorticity, and the flow is divergent away from the lower horizontal boundary; a separation of flow occurs on the bottom near the lower corner. These have been studied experimentally as well in finite cavities by Bejan, Al-homond and Imberger [2], and more recently transient features of the motion for high Rayleigh numbers in a square cavity have been investigated in [14], [17], and [15]. But for the region  $R_1 = R/L = O(1)$ , the jet-like structure and the separation flow are observed numerically here for the first time. According to present numerical results, the flow separation should first occur around  $25000 < RI \leq 40,000$ . Obviously, at present, there are no experiment results available for this case. Some analytical results will provide a comparison to a certain extent, but a precise comparison is not available. Further properties of the flow are displayed in Figures 6, 7, and 8. In Figure 6, the temperature indicates two distinct flow regions: the thin boundary layer region and the parallel core region. The skin friction also shows the complex end region and the core region, The skin friction curve gives a clear picture of the strong vorticity source zone and the flow separation zone. The complication of the flow is also shown in the velocity field. Figure 7 gives the vertical



velocity at various position of  $z$ . The  $z = 0.0625$  (dashed line) curve displays the upstream and the downstream flow near the cold wall, which corresponds to the reverse flow on the bottom. The  $z = 0.2188$  (solid line) curve shows that the flow is influenced by the multiple-eddy structure, and that the velocity has multiple local minimum and maximum values. At  $z = 0.5156$  (dotted line), the boundary layer structure and the core structure are clearly distinguished. In Figure 8, horizontal velocity is displayed at various locations of  $z$ . At  $z = 0.2344$  (dashed line), the eddy structure near the bottom area of the cavity, and at  $x = 0.4687$  (solid line), the reverse flow at the bottom is visible. At  $z = 0.625$  (dotted line), the fluid travels to the cold wall through the upper part of the cavity and travels back to the hot wall through the lower part of the cavity. It is easy to note that the most complicated flow pattern is located in  $0.0 \leq x \leq 1.0$ , and this square area indicates various flow phenomena.

## 5 The evolution of time-dependent, flow

Recently, the time dependent flow in thermally-driven cavities has attracted wide attention due to many geophysical and industrial applications. Patterson and Imberger [16] carried out one of the first investigation of the transient flow in a rectangular cavity, in which a theoretical and computational investigation identified many of the important length, time and velocity scales of the flow, allowing a classification of the various possible flow regions. A number of interesting features were revealed, including an oscillatory approach to steady state under certain conditions. Ivey [14] carried out a series of experiments designed to test for the existence of the oscillatory behaviour, and evidence of the oscillations was found. Schladow, Patterson and Street [18] performed more detail numerical simulations of the Ivey experiment. Their results showed the oscillatory behaviour in the net Nusselt

number, and supported the conclusions of [16]. In contrast, there has been comparatively little work on the time-evolution of flows in shallow cavities where  $L \gg 1$ . One of the first rational investigations of the evolution of thermally driven shallow cavity flows was carried out by Daniels and Wang [9]. There they discussed the evolution of the flow with a certain class of initial conditions both analytically and numerically. But for high Rayleigh number flows more work on the evolution needs to be considered. The present study focuses on a high Rayleigh number evolution flow which starts from a steady state solution of a lower  $R_1$ . Numerical results are presented as following.

Figure 9 shows the streamline of  $R_1 = 40,000$  with  $0 \leq t \leq 0.733$  at a different time level and the steady state solution of  $R_1 = 25,000$  was used for an initial condition. It is interesting to note that at an early time  $t = 8 \times 10^{-3}$  the end zone is filled with a strong nonlinear flow. But with the increasing of time, the perturbations decay on the horizontal intrusion before the far wall is reached and eventually die away when the flow approaches the final steady state. These behaviors appear to be of similar character to those observed by setting an initial profile of the form

$$\tilde{T} = \left(1 - \frac{a}{L}\right) \frac{x}{L} + \frac{a}{2L}, \quad \tilde{\psi} = 0 \quad \text{at} \quad t = 0 \quad (21)$$

with  $a = 4$  discussed in [9]. But here it must be noted that these waves were not generated by either the flow initiation or the impact of the intrusion, and are due to increasing the Rayleigh number instantaneously. At  $t \rightarrow \infty$ , the waves will not propagate over the length of the cavity but will decay as they travel horizontally. In Figure 10, the vertical velocity field at  $z = 0.5$  is illustrated in time, and it is clear that it is disturbed by the occurrence of perturbations due to the sudden increase of Rayleigh number and has an oscillatory behaviour around  $0 \leq x \leq 3$ . The influence of traveling instabilities is obvious at the early time, and this phenomenon disappears as  $t \rightarrow \infty$ . But the properties of the instability of the boundary layer and the flow separation exist during the whole

evolution of flow, and those features are determined by Rayleigh number  $R_1$ , Prandtl number  $\sigma$ , and the aspect ratio  $L$ . The initial set up significantly influences flow structure during the transition. The local Nusselt numbers  $Nu = \frac{\partial T}{\partial x}$  on the cold wall and on  $x = 0.5$  are illustrated in Figures 11 and 12 respectively. On the cold wall, since the strong temperature gradient is set up at the upper corner, the most contribution for local Nusselt numbers comes from the upper region, and decreases as  $z$  tends to zero. But at  $x = 0.5$ , a sharp temperature gradient is set up at  $0.2 < z < 0.3$ , which exhibits jet-like behaviour in regions at the bottom of the cold wall ( and the top of the hot wall) where fluid descending (or ascending) in a vertical boundary layer penetrates into the core.

## 6 Conclusions

in this paper, a detailed numerical study of the end zone in a shallow cavity with insulated horizontal boundaries has been described for higher Rayleigh number flows. For steady state flows, a single eddy near the lower corner occurs around  $R_1 \approx 6000$ , and multiple eddies are formed near the cold wall around  $R_1 \approx 25000$ . A jet-like motion appears when Rayleigh numbers go higher, and eventually at  $R_1 \approx 40000$  flow separation is observed on the bottom near the cold wall. All of these features in the end zone indicates that the flow there is connectively-dominated, and that the boundary layer instability exists at large Rayleigh numbers. This boundary layer instability is of fundamental importance in the development of the flow in the next stage. For the time-dependent flow, strong nonlinearities are immediately observed for a relatively large area near the cold wall after the flow starts from a steady state solution of a lower Rayleigh number. Travelling waves are generated near the cold wall and as  $t \rightarrow \infty$  these waves decay away and eventually die when the steady state is reached. In the future we hope to use a fast parallel adaptive composite multigrid

method in a parallel computing environment for modelling large Rayleigh number convective flows in three dimensions, which will give a better approximation of a real flow problem.

## **7 Acknowledgments**

The research described in this paper was carried out by the Jet Propulsion Laboratory, California Institute of Technology, and was sponsored by the National Research Council and the National Aeronautics and Space Administration while one of the authors (P. Wang) held a NRC-J PI, Research Associateship.

Reference herein to any specific commercial product, process, or service by trade name, trademark, manufacturer, or otherwise, does not constitute or imply its endorsement by the United States Government, the National Research Council, or the Jet Propulsion Laboratory, California Institute of Technology.

This research was performed in part using the CSCC parallel computer system operated by Caltech on behalf of the Concurrent Supercomputing Consortium. Access to this facility was provided by NASA.

The Cray Supercomputer used in this investigation was provided by funding from the NASA Offices of Mission to Planet Earth, Aeronautics, and Space Science.

Access to the Intel Paragon at the Jet Propulsion Laboratory, California Institute of Technology, was provided by the NASA High Performance Computing and Communications Office.

## **References**


- [1] A. Arakawa. Computational design for long-term numerical integration of the equations of fluid

motion: Two dimensional incompressible flow, part 1. *J.Comp.Phys.*, **1:119-143**, 1966.

- [2] A. Bejan, A.A. Al-Homoud, and J Imberger. Experimental study of high Rayleigh number convection in a horizontal cavity with different end temperatures. *J.Fluid Mech.*, 109:283-299, 1981.
- [3] A. Brandt. Multi-level adaptive solutions to boundary-value problems. *Math. Comp.*, 31:333-390, 1977!
- [4] A. Bejan and C. L. Tien. Laminar natural convection heat transfer in a horizontal cavity with different end temperatures. *Trans.A. S.M.E. : J. Heat Trans*, 100:641-647, 1978,
- [5] P.G.Daniels. High Rayleigh number thermal convection in a shallow laterally heated cavity. *Proc.Roy. Soc.A*, 411:327-289, 1993.
- [6] P. G. Daniels and R.J. Gargaro. Numerical and asymptotic solutions for the thermal wall jet. *J. Eng.Math.*, 26:493-508, 1992.
- [7] P. G. Daniels and R.J.Gargaro. Buoyancy effects in stably-stratified horizontal boundary-layer flow. *J. Fluid Mech.*, 250:233-251, 1993.
- [8] J.E.Drummond and S.A.Korpela. Natural convection in a shallow cavity, *J, Fluid Mech.*, 182:543-564, 1987.
- [9] P.G. Daniels and P. Wang. On the evolution of thermally-driven shallow cavity flows. *J. Fluid Mech.*, 259:107-124, 1994.
- [10] P.G.Daniels, P.A.Blythe, and P.G. Simpkins. Onset of multicellular convection in a shallow laterally heated cavity. *Proc.Roy. Sot. A*, 411:327-350, 1987.

- [1] A. E. Gill. The boundary-layer regime for convection in a rectangular cavity. *J. Fluid Mech.*, **26:515-536**, 1966.
- [12] J. E. Hart. Stability of thin non-rotating Hadley circulations. *J. Atmos. Sci.*, 29:687-697, 1972.
- [13] J. E. Hart. Low Prandtl number convection between differentially heated end walls. *Int. J. Heat Mass Transfer*, 26:1069-1074, 1983.
- [14] G. N. Ivey. Experiments on transient natural convection, in a cavity. *J. Fluid Mech.*, 144:389-401, 1984.
- [15] J. C. Patterson and S. W. Armfield. Transient features of natural convection in a cavity. *J. Fluid Mech.*, 219:469-497, 1990.
- [16] J. C. Patterson and J. Imberger. Unsteady natural convection in a rectangular cavity. *J. Fluid Mech.*, 100:65-86, 1980.
- [17] P. G. Simkins and K. S. Chen. Convection in horizontal cavities. *J. Fluid Mech.*, 166:21-39, 1986.
- [18] S. G. Schladow, J. C. Patterson, and R. I. Street. Transient flow in a side-heated cavity at high Rayleigh number: a numerical study. *J. Fluid Mech.*, 200:121-148, 1989.
- [19] P. Wang. *Thermal Convection in Slender Laterally-Heated Cavities*. Ph.D Dissertation, City University, London, 1992.
- [20] P. Wang and P. G. Daniels. Numerical solutions for the flow near the end of a shallow laterally heated cavity. *J. Eng. Math.*, 28:211-226, 1994.



- 
- [21] P. Wang and P.G.Daniels. Numerical study of thermal convection in shallow cavities with conducting boundaries. *Int. J. Heat Mass Transfer*, 37:375-386, 1994.
- [22] P. Wang and P. D. Ferraro. Parallel computation for natural convection. *Concurrency Practice and Experience*. Submitted, 1995.

## List of Figures

1. An example of a  $\text{mesh}$  partitioned among 4 processors (nodes) of a parallel computer.
2. Contours of the steady-state solution for (a) stream function , (b) vorticity, (c) temperature, for  $\sigma = 0.733$  and  $R_1 = 6000$ , using a  $1024 \times 64$  computational grid with  $x_\infty = 16$ .
3. Contours of the steady-state solution near the cold wall for (a) stream function , (b) vorticity, (c) temperature, for  $\sigma = 0.733$  and  $R_1 = 10000$ , using a  $1024 \times 64$  computational grid with  $x_\infty = 16$ .
4. Contours of the steady-state solution for (a) stream function , (b) vorticity, (c) temperature, for  $\sigma = 0.733$  and  $R_1 = 40000$ , using a  $2048 \times 64$  computational grid with  $x_\infty = 32$ .
5. Contours of the steady-state solution near the cold wall for (a) stream function , (b) vorticity, (c) temperature, for  $\sigma = 0.733$  and  $R_1 = 40000$ .
6. The profiles of temperature  $T'$  and skin friction  $\omega/R_1 \times 10^2$  with  $\sigma = 0.733$  and  $R_1 = 40000$  on the bottom.
7. The profile of vertical velocity  $w$  at different positions of  $z$  with  $\sigma = 0.733$  and  $R_1 = 40000$  on the bottom.
8. The profile of horizontal velocity  $u$  at different positions of  $x$  with  $\sigma = 0.733$  and  $R_1 = 40000$  on the bottom.

9. Contours of the time-dependent solution for stream function, with  $\sigma = 0.733$  and  $R_1 = 40000$

near the cold wall at (a)  $t = 0.008$ , (b)  $t = 0.024$ , (c)  $t = 0.2$ , (d)  $t = 1.04$ , and (e)  $t = 1.67$ .

The steady state solution of  $R_1 = 25000$  was used as an initial condition.

10. The local Nusselt number  $\partial T / \partial x$  with  $\sigma = 0.733$  and  $R_1 = 40000$  for different time levels on the cold wall,

11. The local Nusselt number  $\partial T / \partial x$  with  $\sigma = 0.733$  and  $R_1 = 40000$  for different time levels at  $x = 0.5$ .

12. The profile of vertical velocity  $w$  for the time dependent solution at  $x = 0.5$ .

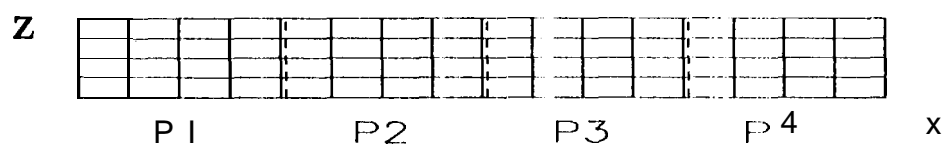
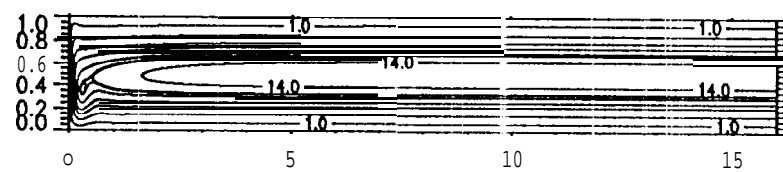
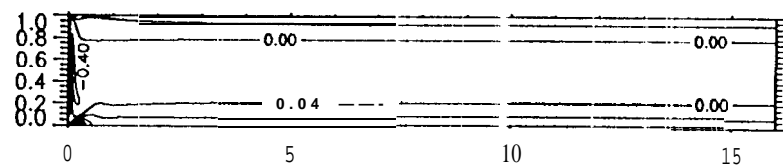


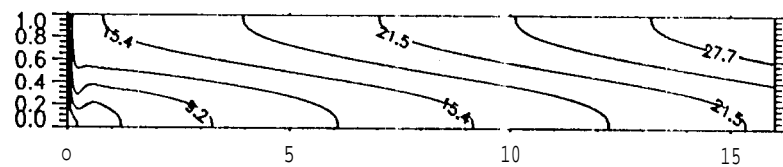
Fig. 1



(a)



(b)

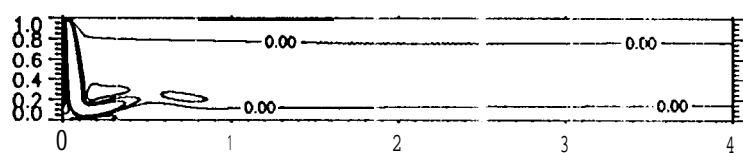


(c)

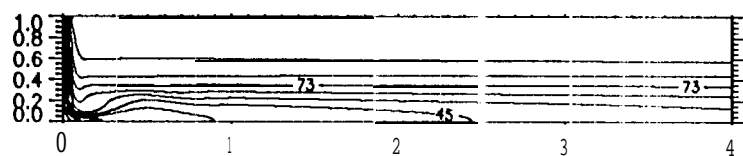
Fig. 2



(a)

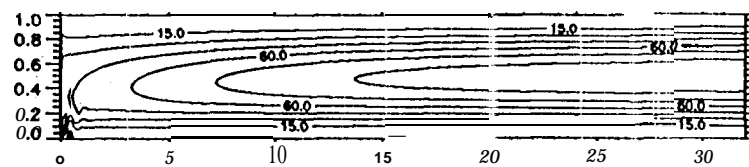


(b)

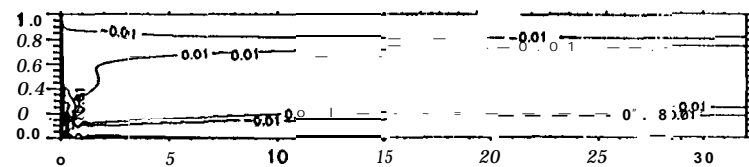


(c)

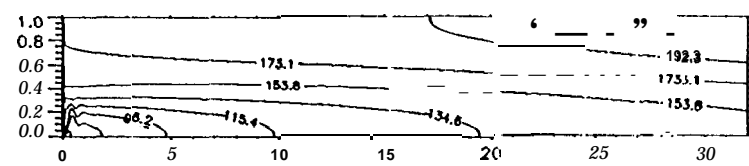
Fig. 3



(a)

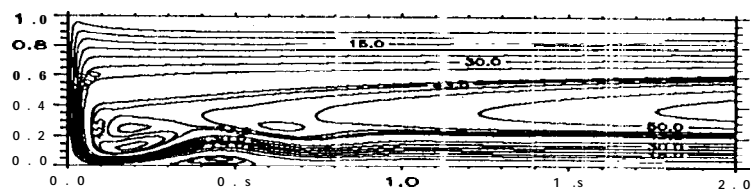


(b)

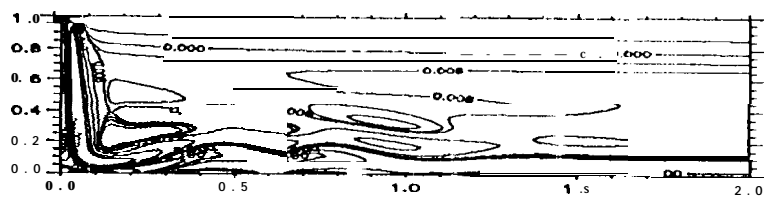


(c)

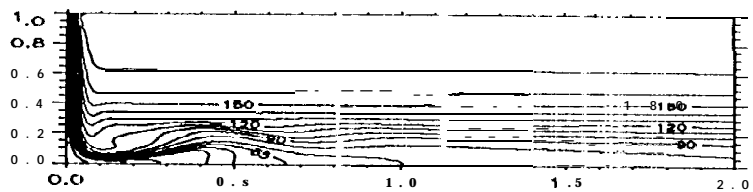
Fig. 4



(a)



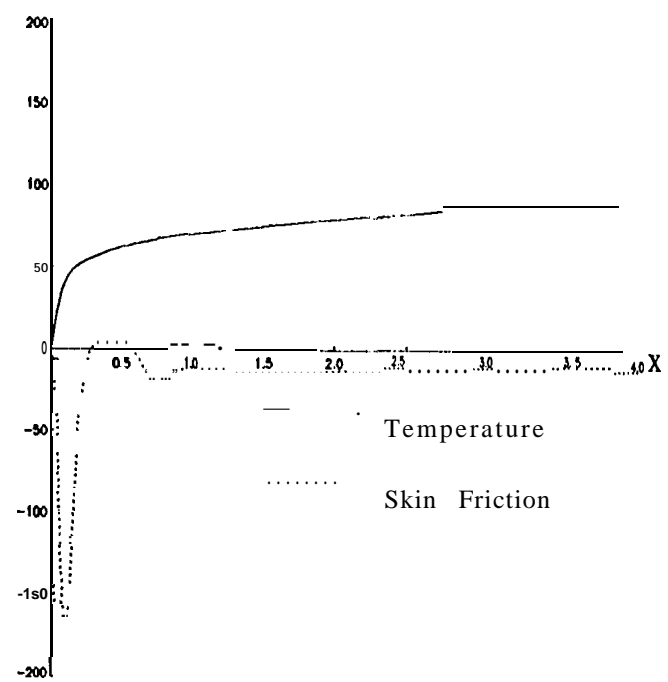
(b)



(c)

Fig. 5





Fig, 6

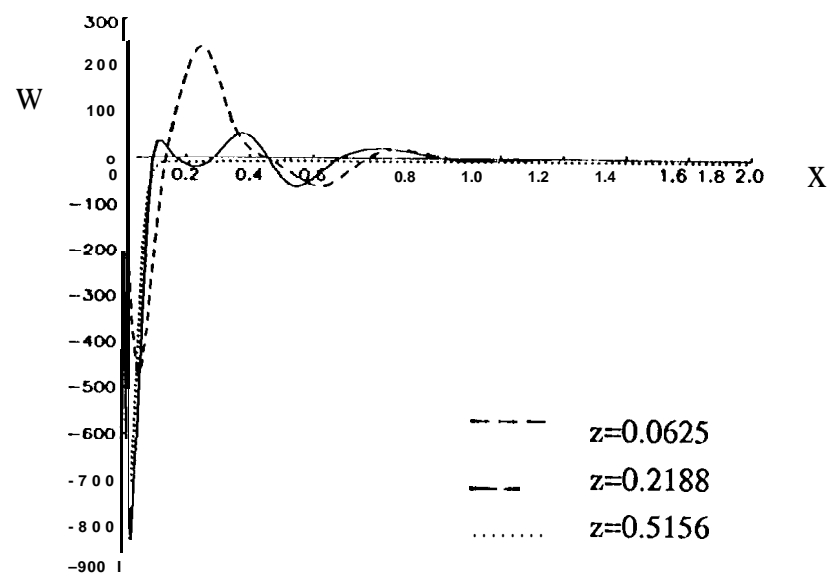


Fig. 7

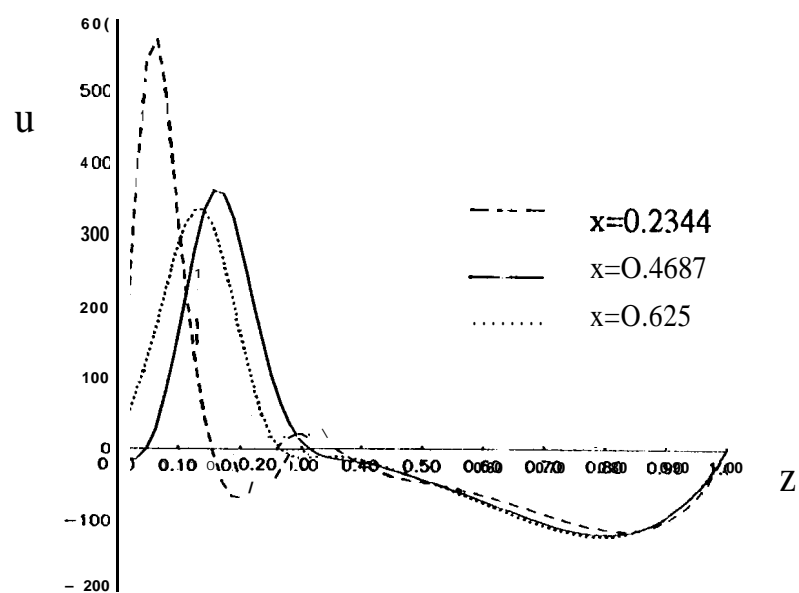


Fig. 8

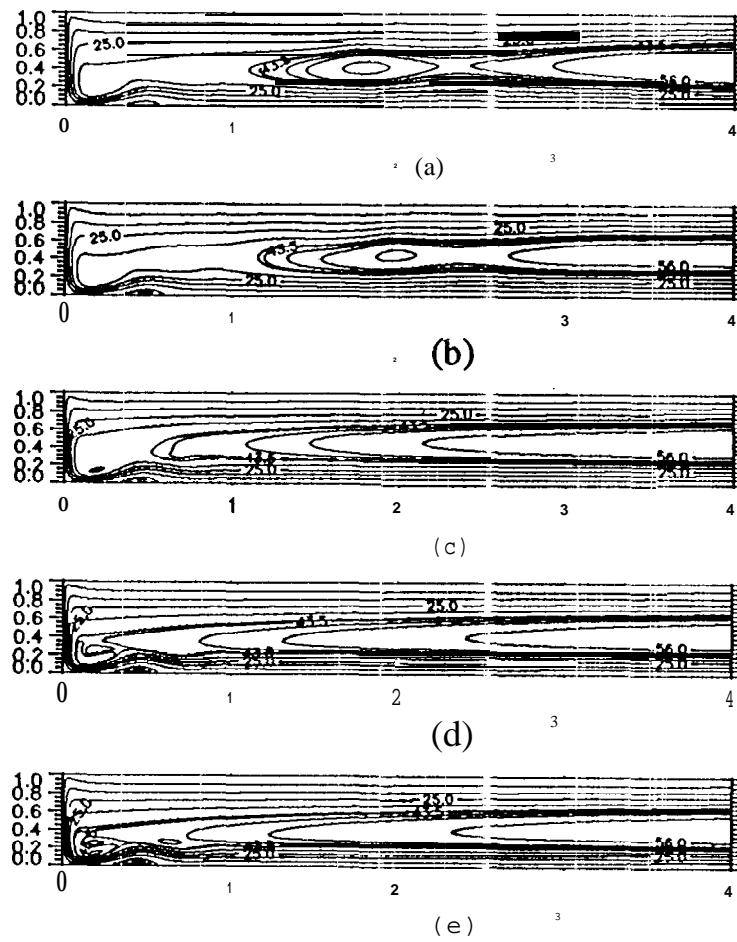


Fig. 9

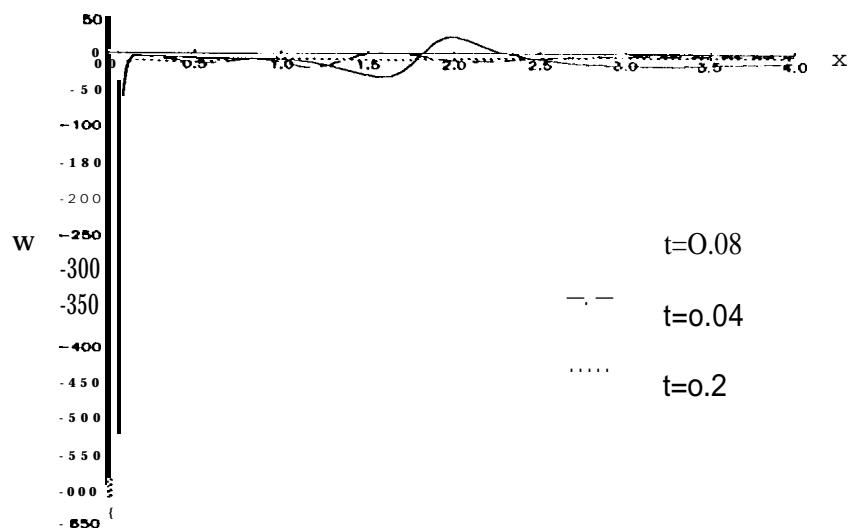


Fig. 10

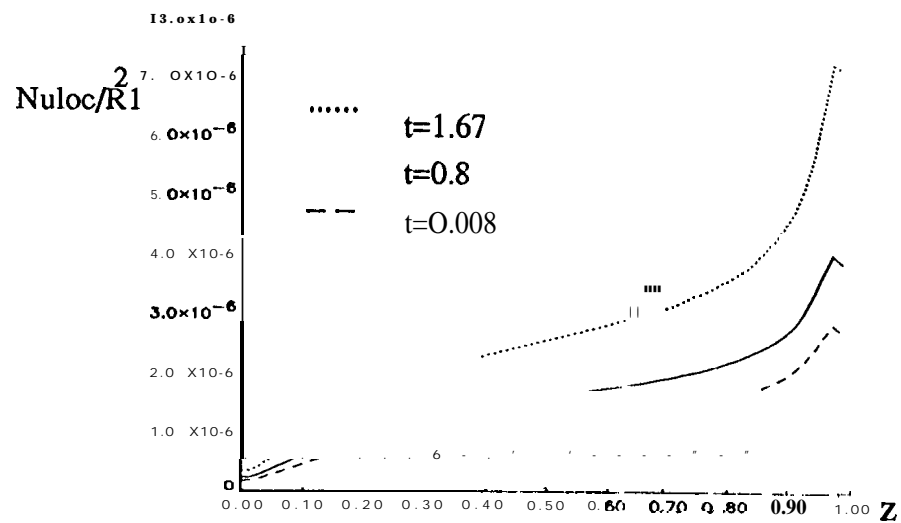


Fig. 11

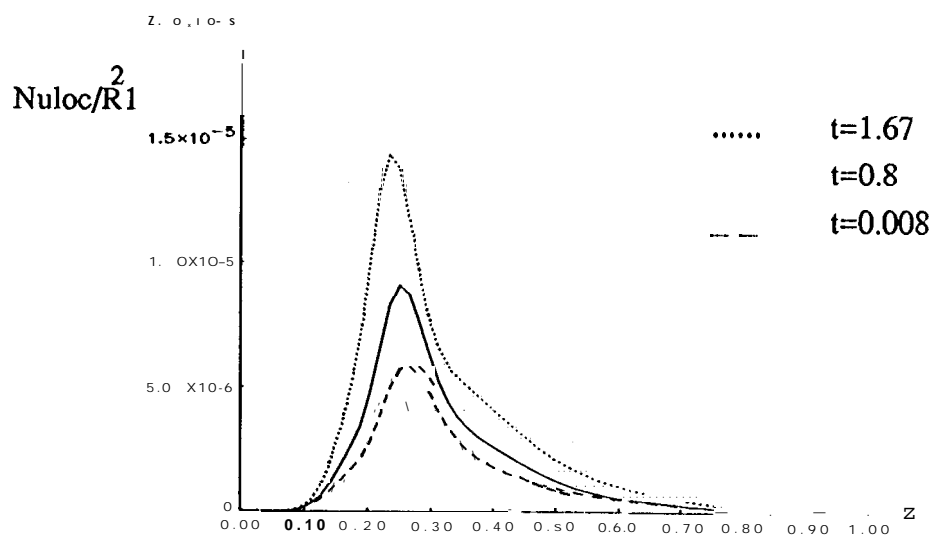


Fig. 12